EXPERIMENTAL AND NUMERICAL FLOW INVESTIGATION OF A CENTRIPETAL SUPERSONIC TURBINE FOR ORGANIC RANKINE CYCLE APPLICATIONS

B. Bülten [1], W. Althaus [1], E. Weidner [1], H. Stoff [2]

[1] Energy Systems Engineering Department, Fraunhofer Institute for Environmental, Safety, and Energy Technology UMSICHT, 46047 Oberhausen, Germany
(bjoern.buelten, wilhelm.althaus, eckhard.weidner)@umsicht.fraunhofer.de

[2] Chair of Thermal Turbomachinery, Ruhr-University Bochum, 44801 Bochum, Germany
(horst.stoff@rub.de)

ABSTRACT

The flow inside a new centripetal supersonic turbine for Organic Rankine Cycle (ORC) applications is investigated. The prototype achieved an isentropic internal efficiency of 64 %. Objectives of this work are the localization and reduction of losses inside the turbine. For this reason a numerical flow simulation is validated with measurements of the prototype. It can be concluded that the model implemented in ANSYS CFX 13.0 reproduces the flow realistically because the deviations of several significant quantities are within the experimental uncertainty. The rotor blades are modified and the supersonic flow deflection is corrected to increase the efficiency. In the numerical simulation the efficiency increases by changing the pitch-to-chord ratio, the flare angle and the flow angle at the outlet of the nozzle blades. The improvements yield a subsequently measured isentropic internal efficiency of about 79 % for the second series of the turbine type.

NOMENCLATURE

A	area	$P_{L,FQ}$	frequency converter loss	ν	velocity ratio
a	speed of sound			Π	pressure ratio
a_b	specific blading work	$P_{L,TC}$	tip clearance loss		
c	absolute velocity	p	pressure	**Subscripts**	
H	height	R	degree of reaction	in	inlet
h	specific enthalpy	T	temperature	liq	liquid
$\dot{m}$	mass flow	u	circumferential speed	out	outlet
Ma	Mach number	$\dot{V}$	volume flow	s	isentropic conditions
N	rotational speed	Z	compressibility factor	t	total conditions
$P_{L,Bear}$	loss in bearings				
$P_{L,CF}$	loss by cross flow	**Greek letters**		**Superscripts**	
$P_{L,DW}$	disc windage loss	α	absolute flow angle	ts	total to static
P_{el}	electrical power	β	relative flow angle	+	nondimensional
$P_{L,Gen}$	generator loss	η_b	blading efficiency		

INTRODUCTION

Industrial processes and small-scale power plants produce a huge amount of waste heat at a high temperature level as a by-product. In many cases this heat is not utilized. One way to recover a part of this waste heat is the application of the Organic Rankine Cycle (ORC) technology. The ORC uses an organic working fluid that is evaporated in a heat exchanger by waste heat and expanded in a turbine. The mechanical power produced by the turbine is converted into electrical power by a generator.

At rated powers above 350 kW$_{el}$ the ORC technology is state of the art. The application of ORCs to rated powers below 350 kW$_{el}$ is still challenging and needs further research and development. One main problem is that there is no efficient and reliable turbine available on the market. Therefore Fraunhofer UMSICHT, Dürr Cyplan and E&P Turbo have developed a small-scale high-temperature ORC with a completely new turbine concept (Althaus et al. 2013). This concept allows cost-efficient manufacturing and easy maintenance due to its compact design and simple construction. The turbine (labeled TG 70, see Figure 1) is a single stage, radial inflow, zero-reaction turbine which is directly coupled with a

Figure 1: Picture of TG 70-Prototype

high-speed generator shaft. The electrical power is fed to the grid by a frequency converter. Methylcyclohexane is used as working fluid and, as far as the authors know, this is the first time in ORC applications. This working fluid leads to a high cycle efficiency and is utilized as lubricant for the bearings, too. Design conditions of the TG 70 are shown in Table 1.

Table 1: Design conditions of the TG 70

P_{el} [kW]	$T_{t,in}$ [°C]	$\Pi = p_{t,in}/p_{out}$ [-]	$\dot{m}$ [kg/s]	N [RPM]
68	243	60	0.75	30000

The turbine is operated in the dense vapor region and expands into the superheated region due to a positive saturation vapor curve. At turbine inlet the compressibility factor Z is about 0.7. Beyond this, speed of sound is low and increases with decreasing temperature at the beginning of the expansion. In a zero-reaction turbine with

$$R_s = \frac{\Delta h_{s,Rotor}}{\Delta h_s} = 0 \tag{1}$$

the entire enthalpy drop happens in the stator vane row. Considering the low speed of sound, the stator vane row has to be designed as a Laval nozzle (a typical Laval nozzle is depicted in Figure 2 at left). To achieve low manufacturing costs a new approach for the design of the Laval nozzle is applied, leading to the geometry shown in Figure 2 at right. In contrast to the typical geometry the convergent-divergent section of the nozzle is turned by 90°. Zero reaction of the turbine leads to supersonic relative velocities at the inlet of the rotor blades. Hence, this turbine is called a supersonic turbine.
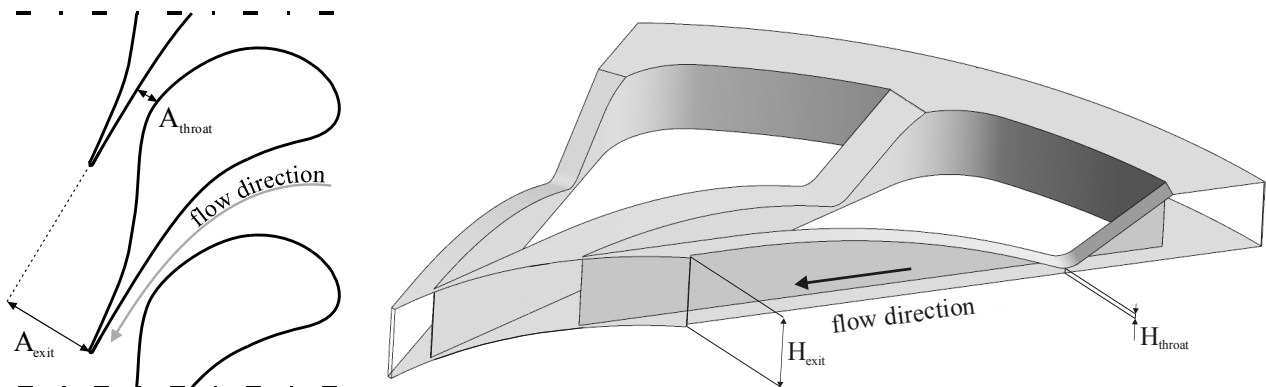

Figure 2: At left, typical Laval nozzle profile, at right, Laval nozzle profile with turned convergent-divergent section

The flow in axial supersonic turbines was investigated experimentally by e.g. Verneau (1987) and Kurzrock (1989) and isentropic internal efficiencies of about 78 % were measured. Supersonic axial turbines are designed for zero reaction, meaning that the pressure is equal at in- and outlet of the rotor blades. The relative velocities at inlet and outlet are almost equal and only the flow direction is changed in the rotor blades. It is called impulse turbine. To reach high efficiencies in supersonic axial turbines special design methods for the stator vanes and rotor blades were adopted (e.g. in Stratford & Sansome, 1960 und Goldman, 1975). In supersonic turbines the incidence of the rotor blade is subject to the 'unique incidence' condition which also determines the pressure at the outlet of the preceding Laval nozzle (Horlock, 1966). If a Laval nozzle is not operated with the design pressure ratio a supersonic flow deflection loss would arise (Stratford & Sansome, 1959 and Verdonk & Dufournet, 1987). Beyond this, a flow separation can occur due to the interaction of the shock wave emanating from the leading edge of the rotor blade and the boundary layer of the suction side (Stratford & Sansome, 1960). The flow in axial supersonic turbines and cascades were simulated by e.g. Rashid et al. (2007), Bassi et al. (1991) and Hefazi et al. (1995) with different solvers. Depending on the turbulence model good agreement with experimental data was obtained.

Research of the flow in radial inflow supersonic turbines was less extensive in the past. In the here introduced concept the radial inflow supersonic turbine is designed for zero reaction. In contrast to axial zero-reaction turbines this does not lead to almost equal relative velocities at in- and outlet of the rotor blades. As the rothalpy stays constant in the rotor blades the relative velocity at the outlet is smaller than at the inlet. Cho et al. (2010) investigated a partial admission, three-stage, radial inflow Curtis-wheel numerically and experimentally and could show that the deviation of the torque is about 5 % using the k-ω-SST model. It is stated that the deviation is caused by the insufficiently accounted partial admission loss in the numerical simulation. Fluid flow in the stator vanes of supersonic radial inflow turbines was investigated in more detail; however the investigations were mainly numerical simulations (e.g. in Reichert & Simon, 1997; Hoffren et al., 2002; Buijtenen et al., 2003; Turunen-Saaresti et al., 2006; Harinck, 2009 and Harinck et al., 2013). An exhaustive comparison with experimental data has not been encountered; solely Turunen-Saaresti et al. (2006) compared the temperature at the outlet of the Laval nozzle and found good agreement using the k-ε model. A flow investigation of radial inflow supersonic rotor blades is missing in the literature until now.

To get a better knowledge of the fluid flow and loss distribution in centripetal supersonic zero-reaction turbines the objectives are (1) numerical and experimental investigation of the new turbine type, (2) validation of the numerical simulation, (3) localization and quantification of the losses and (4) increase of the efficiency. In this article the main results are presented. A more detailed analysis is carried out in Bülten (2014).

EXPERIMENTAL SETUP

The investigated turbine is part of a high temperature ORC which utilizes the exhaust-gas heat of a biogas piston engine. Turbine and generator are hermetically sealed in the same housing with only statically loaded sealings. For the evaluation of the turbine performance the following measuring devices were installed:

- Pressure and temperature at inlet ($p_{t,in}$ and $T_{t,in}$) and outlet (p_{out} and T_{out}) of the turbine,
- Volume flow $\dot{V}_{liq}$ of the liquid phase and temperature of the liquid T_{liq} at outlet of the feed pump of the cycle and
- Electrical power P_{el} and rotational speed N.
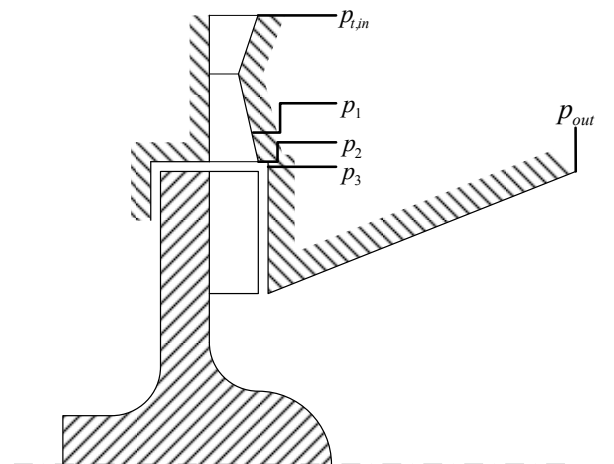

Figure 3: Locations of pressure taps

Pressure taps were added in the expansion path of the turbine (see Figure 3). Two pressure taps are located in the divergent part of the Laval nozzle (p_1 and p_2) and one tap is located in the radial gap between stator vanes and rotor blades (p_3). With these measuring locations it is possible to monitor the flow expansion in the Laval nozzle and to improve the validation of the simulation.

Different operating points were adjusted due to different load conditions of the biogas piston engine which supplies waste heat to the ORC and due to varying ambient temperatures which influence the back pressure. Operating data were plotted every 10 seconds over a time period of 2.5 months. Based on this data stationary operating conditions were generated with a regression analysis (for details see Grob, 2013). A multi-parameter equation of state (MPEOS) developed by Lemmon (2007) was used for the evaluation of the experimental data. The EOS is implemented in Refprop 9.1 (Lemmon et al., 2013). With blading efficiency η_b^{ts} as defined in Craig & Cox (1971) the performance map of the turbine is expressed by:

$$\frac{\dot{m} \cdot \sqrt{T_{t,in}}}{p_{t,in}}, \eta_b^{ts} = \frac{a_b}{\Delta h_s^{ts}}, \frac{\dot{m} \cdot a_b}{p_{t,in} \cdot \sqrt{T_{t,in}}} = f\left(\frac{N}{\sqrt{T_{t,in}}}, \nu = \frac{u}{c_s}\right) \tag{2}$$

Mass flow is calculated by $\dot{m} = \rho(p_{t,in}, T_{liq}) \cdot \dot{V}_{liq}$. In general the isentropic internal efficiency of a turbine can be calculated over the measurements of pressure and temperature at inlet and outlet. However, due to the compact design of the turbine and a manufacturing imperfection of a detail of the interspace between bearing and rotor casing chamber cross flows occurred. These cross flows interacted with the rotor and the temperature sensor at the outlet. Therefore the efficiency could only be calculated by using the measured electrical power P_{el}. To calculate blading work the losses in frequency converter $P_{L,FQ}$, generator $P_{L,Gen}$ and bearings $P_{L,Bear}$ as well as the tip clearance $P_{L,TC}$ and disc windage losses $P_{L,DW}$ have to be accounted for. Furthermore the loss due to the cross flows between bearing and casing chamber of the rotor $P_{L,CF}$ has to be calculated. This leads to:

$$a_b = \frac{1}{\dot{m}} \cdot \left(P_{el} + P_{L,Bear} + P_{L,Gen} + P_{L,FQ} + P_{L,TC} + P_{L,DW} + P_{L,CF}\right) \tag{3}$$

As the measurement of these individual losses is not possible because of cross flows and heat conduction in the turbine the calculation is partially based on the manufacturer's information. Losses in frequency converter, generator and bearings were given by the manufacturer of the turbine. To calculate the tip clearance loss a correlation of Moustapha & Zelesky (2003) for shrouded axial turbines was used since no correlation for shrouded radial inflow zero-reaction turbines was found in literature. Calculations of the disc windage loss with a model of Schlichting & Gersten (1997) showed that this loss is very small and therefore it was neglected. To calculate the cross-flow loss it is assumed that the fluid arriving from the bearing is accelerated by rotor rotation to the tip speed of the rotor. To accomplish this acceleration the rotor is performing work on the fluid. The mass flow of this fluid is calculated according to geometry conditions at the outlet of the bearing. The loss is then calculated by:

$$\Delta P_{L,CF} = \dot{m}_{CF} \cdot \frac{u_{tip}^2}{2} \tag{4}$$

NUMERICAL SETUP

Numerical model and mesh generation

The three-dimensional numerical viscous flow simulations were conducted with the commercial CFD Code ANSYS CFX 13.0. In CFX several options for fluid flow modeling and discretization of

the equations are available. Concerning this work the most important settings – which are not default – are summarized in Table 2. For detailed information it is referred to ANSYS CFX (2010).

Table 2: Executed settings in ANSYS CFX 13.0

Advection term	Specified blend factor β=1
Turbulence model	Standard k-ε or k-ω-SST model with: • Compressible production • Curvature correction • Kato-Launder modification
Equation of state	Implementation of Real-gas EOS with look-up table
Further settings	Stationary simulation Double precision Include viscous work term in energy equation High speed numerics (velocity pressure coupling is modified near shocks)
Convergence criteria for all equations	Max. residuals $\leq 3*10^{-4}$, RMS residuals $\leq 10^{-5}$ Domain imbalance $\leq 10^{-1}$ Monitor points (local and global values) are const.

Periodically symmetric grids were constructed for Laval nozzles, rotor blades and diffusor with mesh expansion ratios below 5 and orthogonality angles (angle between adjacent element edges) above 20°. Taking into account the different turbulence models used in this investigation and their respective near wall treatment, two different grids for each component were created: One grid with y^+_{max}=30 used for simulations with the *k-ε* model and one grid with y^+_{max}=1 for simulations with the k-ω-SST model. Grid refinement studies were conducted for each component leading to grid sizes of 1.5 M. (Laval nozzle), 1 M. (rotor blade) and 1.8 M. (diffusor) in the case of a grid with y^+_{max}=30. Meshes of Laval nozzle and rotor blade are shown in Figure 4.
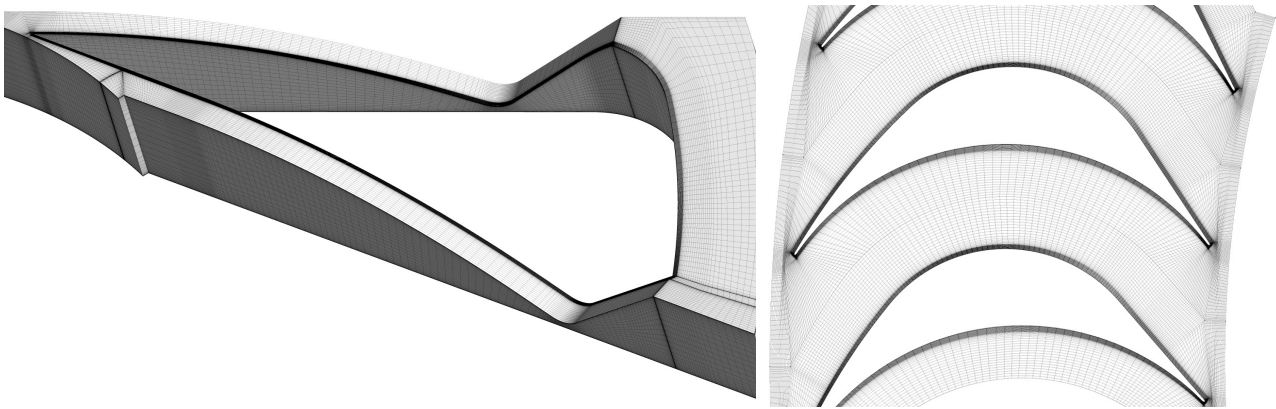

Figure 4: At left, mesh of Laval nozzle, at right, mesh of rotor blade

Fluid domain, boundary conditions and domain interfaces

The fluid domain contains stator vanes, rotor blades and diffusor (see Figure 5 at left). It is assumed that the flow field is rotationally symmetric. With this assumption it is possible to simulate only a segment of the whole turbine, reducing the simulation time significantly. To avoid recirculating flow at the outlet of the domain the diffusor was extended axially. At the inlet of the concentrically arranged Laval nozzles total pressure and total temperature were specified whereas the average static pressure was set at the outlet of the domain. The flow was treated as adiabatic. At the walls the no-slip condition was adjusted. Between Laval nozzles and rotating rotor blades a mixing plane was placed. A frozen rotor interface was located between rotor blades and diffusor.

Data reduction

The nonuniform three-dimensional flow field has to be averaged at certain locations to analyze the fluid flow in the turbine. Therefore several averaging planes – which are shown in Figure 5 at

right – were added in the post processor. Blading efficiency and pressure ratio were calculated over turbine inlet and averaging plane E at the diffusor outlet (not domain outlet). Overall losses can be subdivided into losses of the single components. Losses in the Laval nozzles were quantified over turbine inlet and averaging plane B. To distinguish between losses in the convergent-divergent part and supersonic flow deflection losses at the nozzle outlet a further averaging plane A was introduced. Losses in the rotor blades were calculated over averaging planes C and D and losses in the diffusor over averaging planes D and E. At these averaging planes total enthalpy and the single velocity components (axial, radial and circumferential) were mass-flow averaged. Static pressure was area averaged. All other values (e.g. static enthalpy and entropy) were calculated on this basis.
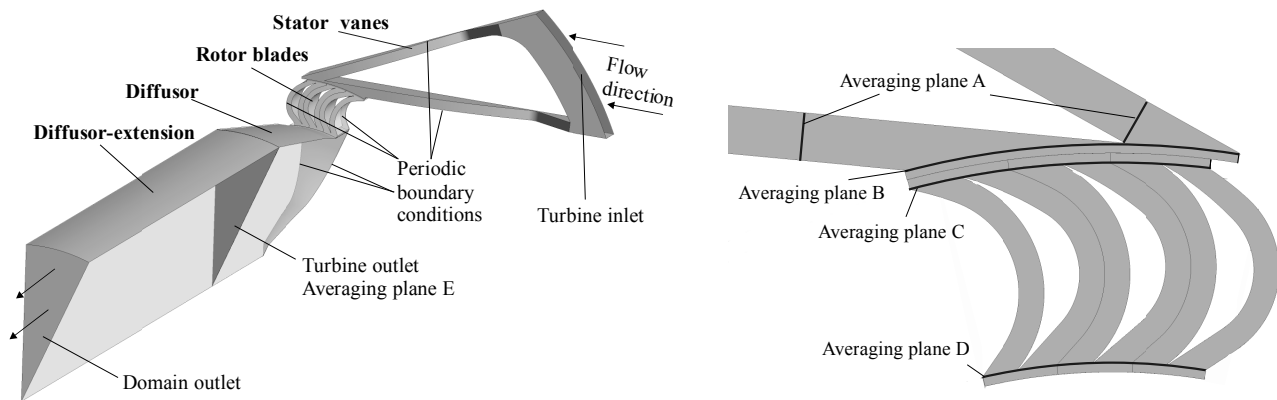

Figure 5: At left, fluid domain, boundary conditions and location of averaging plane at turbine outlet, at right, locations of averaging planes in stator vanes and rotor blades

RESULTS

Flow field and loss distribution

To get an overview of the flow field and the loss distribution the flow was numerically investigated at the operating point with the highest efficiency. The pressure gradient at mid-span of Laval nozzles and rotor blades is depicted in Figure 6 at left for simulations with the k-ε model.
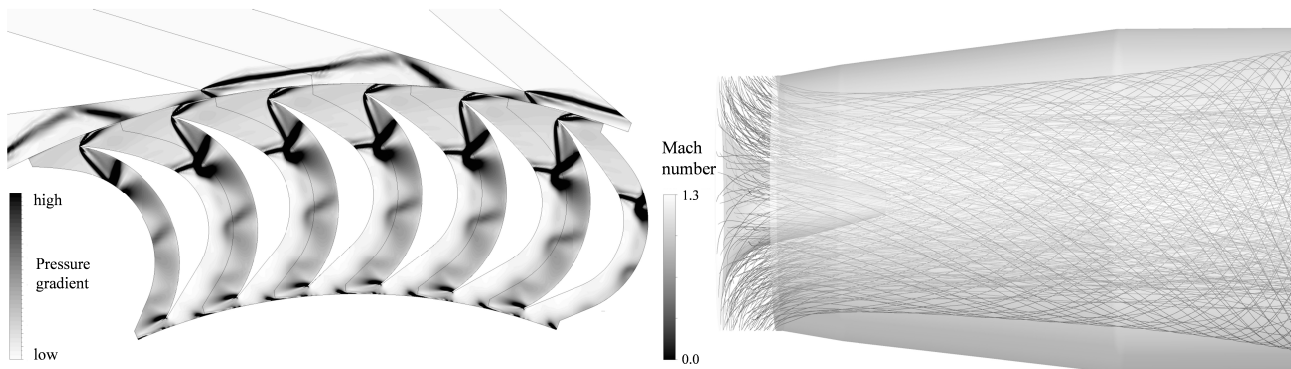

Figure 6: At left, Pressure gradient at mid-span in Laval nozzles and rotor blades at the operating point with highest efficiency (k-ε model), at left, Mach number streamlines in diffusor at the operating point with highest efficiency (k-ε model)

At the exit of the divergent section of the Laval nozzles the fluid has a Mach number of about 3. Since the nozzle is not operated at design pressure ratio and the mean line of the profile is straight an oblique shock wave occurs at the Laval nozzle outlet leading to a compression and a deceleration of the flow. The pressure at the Laval nozzle outlet is controlled by the 'unique incidence' condition, the rotating speed and the conservation of angular momentum in the radial gap. A relative Mach number at rotor blade inlet of about 1.6 leads to an oblique shock wave emanating from the leading edge. Due to the curvature of the pressure side a coalescing normal shock occurs which

interacts with the boundary layer of the suction side. This leads to a flow separation. This coalescing normal shock and the induced flow separation were verified in turbine cascades by Tanaka et al. (1984) and Stratford & Sansome (1960). The normal shock decelerates the flow to subsonic velocities. Downstream the flow is accelerated and decelerated repeatedly. Since the flow separation extends over the entire suction side the fluid flow cannot follow the blade contour at outlet of the rotor blades. This leads to increased exit swirl. Mach number streamlines in the diffusor are shown in Figure 6 at right. Due to the centripetal inlet and the large opening angle of the diffusor the flow separates at the outer wall.

Loss distribution at the operating point with highest efficiency for simulations with the k-ε model is shown in Figure 7. The isentropic enthalpy drop is divided into useful blading work and losses. Losses are further contributed to the components where the losses occur. The highest losses are generated in the Laval nozzle due to friction. Additionally a supersonic flow deflection loss arises since the Laval nozzle is not operated with design pressure ratio. The flow inside the radial gap could be considered as almost isentropic. Reasons for the rotor blade losses are the normal shock waves and the flow separation at the suction side. Due to the flow separation the flow leaves the rotor blades with swirl which increases the exit velocity. On the one hand this kinetic energy is dissipated in the diffusor and on the other hand it leaves the diffusor. Due to a separation in the diffusor the flow is not diffused but accelerated, leading to a pressure loss. The flow field and loss distribution are similar using the k-ω-SST or k-ε model.
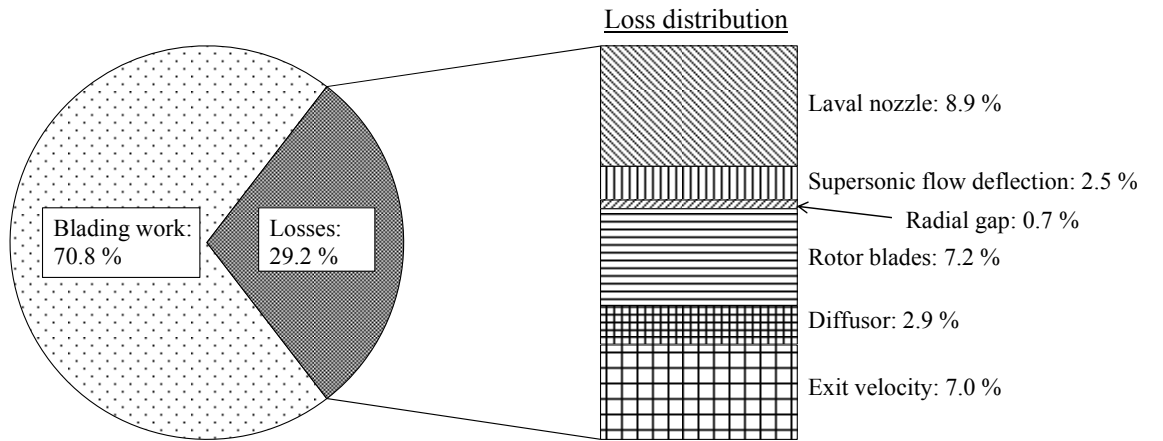

Loss distribution

Blading work: 70.8 %

Losses: 29.2 %

Laval nozzle: 8.9 %

Supersonic flow deflection: 2.5 %

Radial gap: 0.7 %

Rotor blades: 7.2 %

Diffusor: 2.9 %

Exit velocity: 7.0 %

Figure 7: Loss distribution at the operating point with highest efficiency (k-ε model)

Comparison of numerical and experimental results

Numerical and experimental results at the operating point with highest efficiency are compared in Table 3. Reduced mass flow, blading efficiency and two pressures inside the Laval nozzles are reproduced by the k-ε model within the experimental uncertainty. Calculations with the k-ω-SST model reproduce reduced mass flow and pressure 2. Pressure in the radial gap is calculated too small with either turbulence model.

Table 3: Comparison of numerical and experimental results at the operating point with highest efficiency shown as deviation from experimental results

Deviation from experimental results	k-ε	k-ω-SST	Exp. Uncertainty
$\left[\left(\frac{\dot{m}\sqrt{T_{t,in}}}{p_{t,in}}\right)_{num} - \left(\frac{\dot{m}\sqrt{T_{t,in}}}{p_{t,in}}\right)_{exp}\right]/\left(\frac{\dot{m}\sqrt{T_{t,in}}}{p_{t,in}}\right)_{exp}$	0.2 %	0.1 %	±1.0 %
$[(\eta_b^{ts})_{num} - (\eta_b^{ts})_{exp}]/(\eta_b^{ts})_{exp}$	3.1 %	4.3 %	±3.2 %
$[(p_1)_{num} - (p_1)_{exp}]/(p_1)_{exp}$	3.1 %	3.9 %	±3.5 %
$[(p_2)_{num} - (p_2)_{exp}]/(p_2)_{exp}$	1.1 %	1.7 %	±4.0 %
$[(p_3)_{num} - (p_3)_{exp}]/(p_3)_{exp}$	-14.1 %	-11.9 %	±3.3 %

For $N/\sqrt{T_{t,in}}$=125 numerical investigations of the part load behavior were conducted with the $k\text{-}\varepsilon$ model and are compared with experimental data in Figure 8. Reduced mass flow, reduced blading power and blading efficiency at part load of the turbine are reproduced within their experimental uncertainty. Reduced mass flow is independent of the velocity ratio which is typical for supersonic turbines. The blading efficiency varies from 69 % to 65 % mainly due to changes of the condenser pressure at part load. Simulations with slightly higher velocity ratios indicate a plateau for the blading efficiency and a maximum efficiency at υ=0.41.
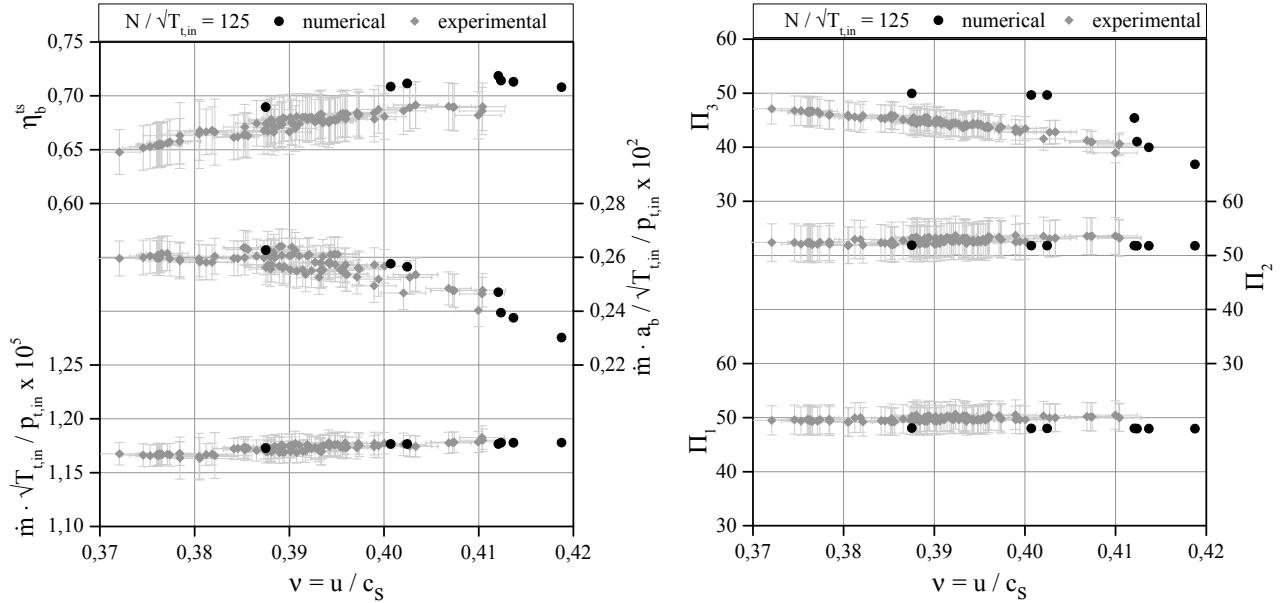

Figure 8: At left, experimentally and numerically determined performance map of the centripetal supersonic turbine, at right, experimentally and numerically determined pressure ratios in the expansion path of the turbine

In Figure 8 at right the pressure ratios $\Pi_j = p_{t,in}/p_j$ of the three measured pressures inside the expansion path (j=1, 2, 3) are depicted. Comparing them with each other it can be seen that the vapor expands in the divergent section ($\Pi_1 < \Pi_2$) and a compression occurs between the exit of the divergent section and the radial gap ($\Pi_2 > \Pi_3$). Pressure ratios inside the divergent section of the nozzle are independent whereas the pressure in the radial gap is dependent on turbine outlet pressure. This may indicate that the flow in the experiments was not started in the rotor blades and the 'unique incidence' does not apply. The numerical simulation is able to calculate the pressures inside the Laval nozzle but the deviation of pressure 3 is larger than the experimental uncertainty. Reasons for this deviation could be that (1) the turbulence model does not reproduce the exact dimensions of the flow separation, (2) the transient effects of the rotor rotation are not taken into account by the mixing plane, (3) the measuring device is not included in the numerical simulation and/or (4) a dynamic pressure caused by the rotation has acted on the pressure transducer.

In summary, the most important characteristic values – namely blading efficiency and reduced mass flow – are reproduced by the numerical simulation.

Analysis of the flow in the rotor blades

Based on the results shown in Figure 8 the flow in the turbine was investigated in more detail with the numerical method. One objective was to determine the rotor blade efficiency as a function of the relative inlet Mach number and the degree of reaction. Therefore further numerical simulations were carried out. In these simulations the inlet conditions of the turbine were kept constant and the rotational speed and the pressure ratio of the turbine were varied. The rotational speed has a direct impact on the relative Mach number at the inlet of the rotor blades. The pressure ratio mainly influences the degree of reaction.
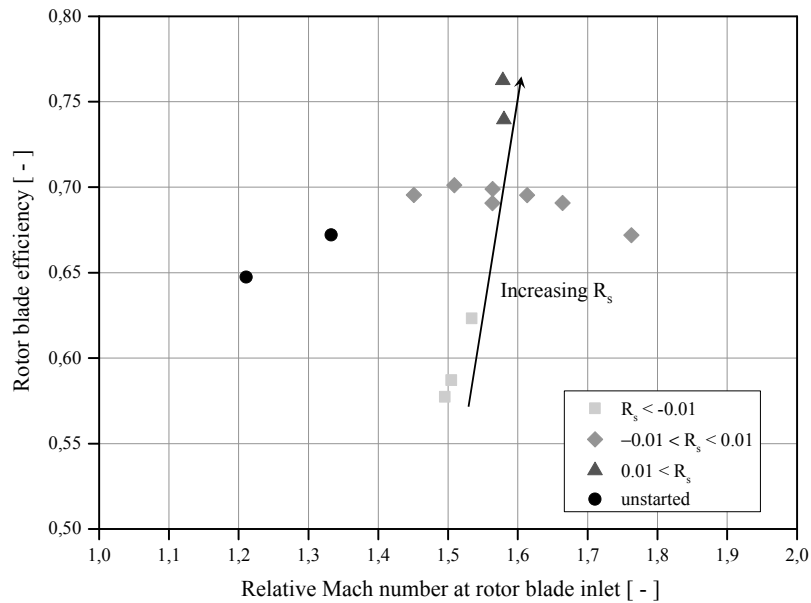
Figure 9: Rotor blade efficiency as a function of the relative inlet Mach number and the degree of reaction

In Figure 9 the rotor blade efficiency is shown as a function of the relative inlet Mach number and the degree of reaction. If the degree of reaction is approximately zero the maximum rotor blade efficiency is about 70 % for a Mach number of about 1,5. With increasing Mach number the flow separation at the suction side gets more severe. A reduced Mach number leads to an unstarted flow with a detached normal shock wave at the leading edge. The rotor blade efficiency drops in either case. If the relative Mach number at the inlet of the rotor blade is kept almost constant (1.5<Ma<1.6), the efficiency rises if the degree of reaction is increased. A higher degree of reaction leads to a reduced flow separation area and to smaller angles of the oblique shock waves (with respect to the flow direction) in the rotor blade passage. A negative degree of reaction results in a detached normal shock wave at the rotor blade inlet and a drop of the rotor blade efficiency.

Efficiency Improvement

In this work only the geometries of stator vanes and rotor blades were modified because these components can be easily replaced in the turbine. In contrast to that the diffusor is welded to a heat exchanger (recuperator) and cannot be modified easily. Because of the large potential for improvement the focus was first set on rotor blade modification. Increasing the efficiency of the rotor blades also means a reduction of the exit swirl, meaning lower exit losses. The main cause for the low rotor blade efficiency is the interaction of the normal shock with the boundary layer of the suction side. Stratford & Sansome (1960) and Tanaka et al. (1984) developed design criteria to prevent the flow separation. In particular the decrease of the pitch-to-chord ratio is fundamental. Beyond this, in Verdonk & Dufournet (1987) and Verneau (1987) it is stated that a low degree of reaction is advantageous for the flow in axial supersonic turbines. A low degree of reaction leads to an accelerated flow in the rotor blades, which is more resistant to flow separations. To achieve an accelerated flow in centripetal turbines the degree of reaction has to be higher than in axial turbines due to the changing circumferential speed. Based on these findings and the results shown in Figure 9 several blade geometries were designed with different pitch-to-chord ratios and varying flare angles. A main constraint for the design was that the geometries still have to be easy to manufacture. In Figure 10 at left the flow field is shown in terms of pressure gradient for the blade profile with the highest efficiency. With this design no coalescing normal shock wave occurs at the pressure side and no flow separation arises. It is avoided because expansion waves of the suction side are interacting with the compression waves of the pressure side and neutralize them. However, at the outlet of the blade profile a small flow separation occurs at the suction side which leads to

further shock waves. Nevertheless, the rotor blade efficiency is increased by 20 % and the flow turning is improved by 2-3 degrees.

To decrease the supersonic flow deflection loss the Laval nozzle should be operated with the design pressure ratio and the radial inflow Laval nozzles should be curved (Reichert & Simon, 1997). However, in this investigation the Laval nozzle profile remains straight because of manufacturing reasons. Nevertheless it is possible to adjust the flow in a way that the nozzle is operated with the design pressure ratio. As stated above the outlet pressure of the Laval nozzle is fixed by the 'unique incidence' condition, the rotating speed and the conservation of angular momentum in the radial gap. Considering this, the numerical results of the rotor blade modification were analyzed in terms of flow angle and pressure distribution at the inlet. With these values pressure and flow angle at the outlet of the Laval nozzles were calculated using the conservation of angular momentum. To adapt the flow angles of Laval nozzles and rotor blades the profile angle of the nozzles (with respect to circumferential direction) was reduced.

Based on the numerical investigation modified geometries for Laval nozzles and rotor blades were manufactured and tested. Results of modified geometry are compared with reference geometry in Figure 10 at right. Blading efficiency of the modified geometry is increased by 17 % to about 81 %. Beyond this, a new design of the interspace between bearing and casing chamber of the rotor minimizes cross flows. This leads to an isentropic internal efficiency of about 79 %.
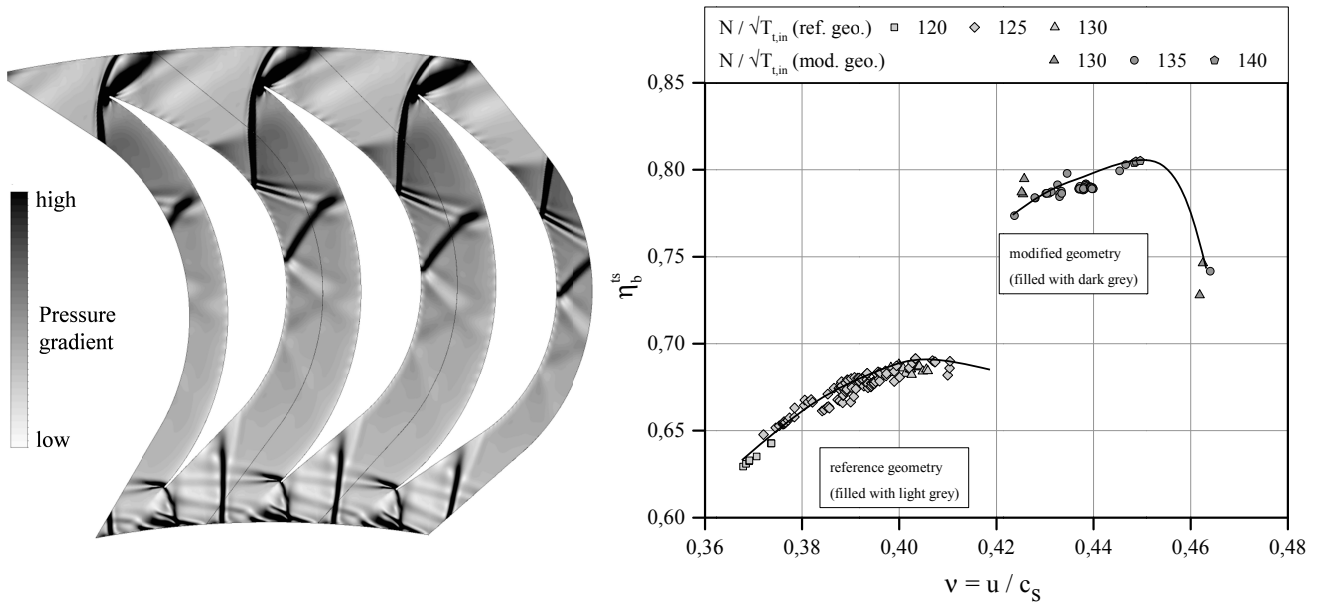

Figure 10: At left, pressure gradient at half-span in modified rotor blade profile, at right, comparison of blading efficiency of reference and modified geometry

CONCLUSIONS

A new turbine type – a centripetal supersonic turbine – is introduced and investigated experimentally and numerically for the first time. It is operated with methylcyclohexane which exhibits real-gas behavior in the dense vapor region. Comparison of experimental and numerical results show good agreement for blading efficiency, reduced mass flow and two pressures inside the Laval nozzle. The main aerodynamic loss mechanisms in the prototype are (**1**) friction losses in the Laval nozzle, (2) a supersonic flow deflection loss at nozzle's outlet, (3) loss due to shock wave boundary layer interaction, leading to a flow separation in the rotor blades, (4) exit loss which is enhanced due to exit swirl and a flow separation at the outer wall of the diffusor. Reduction of the supersonic flow deflection loss, the rotor blade loss, the exit loss and the loss due to cross flows between bearing and rotor leads to an isentropic internal efficiency of 79 %.

However, cross flows inside the turbine have complicated the experimental investigation. For this reason assumptions had to be made for the losses of several components to calculate the blading

efficiency. As the turbine is not operated on a test bench but at a customer site it was not possible to validate these assumptions. Quantification of losses in bearing, generator and frequency converter as well as the cross flow loss should be done by e.g. investigating the turbine on a test bench in future. With better quantified losses the numerical results could be further validated. Beyond this, the tip clearance flow should be considered in the numerical simulation.

Potential for aerodynamic optimization is given for all components. It was found in Reichert & Simon (1997) that a curved mean line of the Laval nozzle leads to an improved efficiency. The rotor blade profile should be optimized to prevent the small flow separation at the outlet. Flow separation in the diffusor could be avoided by e.g. a multi-channel diffusor.

ACKNOWLEDGEMENTS

REFERENCES

Althaus, W.; Paucker R.; Grob, J.; Bülten, B.; Hunstock, B.:*ORC-Prozesse zur Abwärmenutzung an BHKW-Motoren: Feldversuch ORC FKZ-Nr.: 0327436C*, Abschlussbericht zum Entwicklungs-/ Demonstrationsprojekt mit Feldversuch, Oberhausen, 2013.

ANSYS CFX Manual Release 13.0, 2010.

Bassi, F.; Osnaghi, C.; Perdichizzi, A.: *Highly Loaded Turbines for Space Applications: Rotor Flow Analysis and Performance Evaluation*. In: Angelino, G.; Luca, L.; Sirignano, W. (Eds.): Modern Research Topics in Aerospace Propulsion, Springer, New York, 1991, p. 329–354.

Bülten, B.: Experimentelle und numerische Untersuchung der Strömung in einer zentripetal durchströmten Überschallturbine für ORC-Anwendungen. PhD thesis, Ruhr-University Bochum, Bochum, 2014.

Buijtenen, J. P.; Larjola, J.; Turunen-Saaresti, T.: Design and Validation of a New High Expansion Ratio Radial Turbine for ORC Application. Proc. 5th ETC, Prague, 2003.

Cho et al. (2010): Cho, C. H.; Cho, S. Y.; Ahn, K. Y.: *A study of partial admission characteristics on a small-scale radial-inflow turbine*. Proc. Inst. Mech. Eng. A J. Power Energy Vol. 224/5, p. 737–748.

Craig, H. R. M.; Cox, H. J. A.: *Performance Estimation of Axial Flow turbines*, Proc. Inst. Mech. Eng. 1970-71, Vol. 185 32/71, p. 407-424.

Goldman, L. J.: *Supersonic Turbines*. In: Glassman, A. (Ed.): Turbine design and application. NASA SP-290 Vol. 3, 1975, p. 1–29.

Grob, J.: Arbeitsmittelauswahl, Messdatenanalyse und Modellüberprüfung eines Hochtemperatur-Organic-Rankine-Cycle. PhD thesis, Ruhr-University Bochum, Bochum, 2013.

Harinck, J.: Super- and Transcritical Fluid Expansions for Next-Generation Energy Conversion Systems. PhD thesis, TU Delft, Delft, 2009.

Harinck, J.; Pasquale, D.; Pecnik, R.; Buijtenen, J. P.; Colonna, P.: *Performance improvement of a radial ORC turbine by means of automated CFD design*. Proc. 10th ETC, Lappeenranta, 2013.

Hefazi, H.; Kaups, K.; Murry, R.: A Computational Study of Flow over A Supersonic Impulse Turbine Blade. AIAA paper 95-2287, 1995.

Hoffren, J.; Talonpoika, T.; Larjola, J.; Siikonen, T.: *Numerical Simulation of Real-Gas Flow in a Supersonic Turbine Nozzle Ring*. J. Eng. Gas Turbines Power Vol. 124/2 (2002), p. 395–403.

Horlock, J. H.: *Axial flow turbines*. Butterworths, London, 1966.

Kurzrock, J. W.: Experimental investigation of supersonic turbine performance. ASME Paper 89-GT-238, 1989.

Lemmon, E. W.: Unpublished Equation of State for Methylcyclohexan, 2007.

Lemmon, E. W.; Huber, M. L.; McLinden, M. O.: *NIST Standard Reference Database 23: Reference Fluid Thermodynamic and Transport Properties-REFPROP, Version 9.1*, National Institute of Standards and Technology, Gaithersburg, MD, 2013.

Moustapha, H.; Zelesky, M. F.: *Axial and radial turbines*, Concepts NREC, White River Junction, VT, 2003.

Rashid, S.; Tremmel, M.; Waggott, J.; Moll, R.: *Curtis Stage Nozzle/Rotor Aerodynamic Interaction and the Effect on Stage Performance*. J Turbomach Vol. 129/3 (2007), p. 551–562.

Reichert, A. W.; Simon, H.: Design and Flow Field Calculations for Transonic and Supersonic Radial Inflow Turbine Guide Vanes. J Turbomach Vol. 119/1 (1997), p. 103–113.

Schlichting, H.; Gersten, K.: *Grenzschicht-Theorie*, Springer, Berlin u. a., 1997.

Stratford, B. S.; Sansome, G. E.: *The performance of supersonic turbine nozzles*. Aeronautical Research Council R & M No. 3273, 1959.

Stratford, B. S.; Sansome, G. E.: *Theory and tunnel tests of rotor blades for supersonic turbines*. Aeronautical Research Council R & M No. 3275, 1960.

Tanaka, M. E.; Kawashima, T.; Isozaki, T.; Takehira, A.: Investigation of the two-dimensional performance of supersonic impulse turbine blade cascades: 2nd Report, Flow and Losses in Blade Passage and Some Design Criteria. JSME Vol. 27/225 (1984), S. 513–520.

Turunen-Saaresti, T.; Tang, J.; van Buijtenen, J.; Larjola, J.: *Experimental and Numerical Study of Real-Gas Flow in a Supersonic ORC Turbine Nozzle*. ASME paper GT2006-91118.

Verdonk, G.; Dufournet, T.: Development of Supersonic Steam Turbine with a Single Stage Pressure Ratio of 200 for Generator and Mechanical Drive. Small High Pressure Ratio Turbines. VKI Lecture Series, Rhode Saint Genese, 1987.

Verneau, A.: *Supersonic Turbines For Organic Fluid Rankine Cycles from 3 to 1300 kW*. Small High Pressure Ratio Turbines. VKI Lecture Series, Rhode Saint Genese, 1987.